Inorg. Chem. **2009**, *48*, 1214−1222

On the Mechanism of Iron(III)-Dependent Oxidative Dehydrogenation of Amines

Juan Pablo Saucedo-Vázquez,[†] Víctor Manuel Ugalde-Saldívar,[†] Alfredo Rubén Toscano,[‡] Peter M. H. Kroneck,[§] and Martha Elena Sosa-Torres*[,†]

Departamento de Química Inorgánica y Nuclear, Facultad de Química, and Instituto de Química, Universidad Nacional Autónoma de México, Ciudad Universitaria, México, D.F. 04510, México, and Fachbereich Biologie, Universität Konstanz, 78457 Konstanz, Germany

Received September 3, 2008

Kinetic and structural data are presented for the iron-promoted dehydrogenation of the amine, $[Fe(III)L^3]^{3+}$ (**1**), $\mathbf{L}^3$ = 1,9-bis(2′-pyridyl)-5-[(ethoxy-2″-pyridyl)methyl]-2,5,8-triazanonane. Spectroscopic and electrochemical experiments under the exclusion of dioxygen helped to identify reaction intermediates and the final product, the Fe(II)-monoimine complex $[Fe(II)L^4]^{2+}$ (**2**), $\mathbf{L}^4$ = 1,9-bis(2′-pyridyl)-5-[(ethoxy-2″-pyridyl)methyl]-2,5,8-triazanon-1-ene. **2** is formed by disproportionation of the starting complex **1** by a three-step reaction mechanism, most likely via ligand-centered radical intermediates. The rate law can be described by the second-order rate equation, $-d[(Fe(III)L^3)^{3+}]/dt = k_{EtO^-}[(Fe(III)L^3)^{3+}][EtO^-]$, with $k_{EtO^-} = 4.92 \pm 0.01 \times 10^4\ M^{-1}\ s^{-1}$ (60 °C, μ = 0.01 M). The detection of general base catalysis and a primary kinetic isotope effect ($k_{EtO^-}{}^{H}/k_{EtO^-}{}^{D} = 1.73$) represents the first kinetic demonstration that the deprotonation becomes rate determining followed by electron transfer in the oxidative dehydrogenation mechanism. We also isolated the Fe(II)-monoimine complex **2** and determined its structure in solution (NMR) and in the solid state (X-ray).

Introduction

The transition metal-promoted oxidation of organic ligands including amines and alcohols has been studied extensively in both chemical and biological systems.[1] Alcohol dehydrogenases (Zn), galactose oxidase (Cu), and amine oxidases (Cu) are prominent enzymes involved in such reactions.[2] High-resolution X-ray structures have been reported for many of these enzymes. However, their mechanism of action is still not well-understood and requires further detailed investigations.[3] In a similar fashion, Fe(III) coordinated to the lysyl ∈-amino residue has been proposed to cause oxidative damage of proteins by dehydrogenation in the presence of hydrogen peroxide.[4] The oxidation of amines will lead to a variety of products, including nitriles, nitro, and carbonyl species formed by a highly reactive imine. The oxidative dehydrogenation of amines and alcohols by their coordinated metal centers, specifically with a variety of monodentate and bidentate ligands, has been described, with ruthenium and osmium being particularly effective[5,6] So far, not much work has been done with multidentate amine ligands. Earlier, in our work on Fe(III) complexes of the amine ligand 1,9-bis(2′-pyridyl)-2,5,8-triazanonane ($\mathbf{L}^1$), we found that the central metal ion can be reduced via oxidation of the ligand. This reaction is accompanied by an increase in size and denticity of the original ligand.[7] On the basis of electrochemical data,

* E-mail: mest@servidor.unam.mx.
† Departamento de Química de Inorgánica y Nuclear, Facultad de Química, Universidad Nacional Autónoma de México.
‡ Instituto de Química, Universidad Nacional Autónoma de México.
§ Universität Konstanz.

(1) Keene, F. R. *Coord. Chem. Rev.* **1999**, *187*, 121.
(2) (a) Whittaker, M. M.; Whittaker, J. W. *Biophys. J.* **1993**, *64*, 762. (b) Mure, M.; Mills, S. A.; Klinman, J. P. *Biochemistry.* **2002**, *41*, 9269. (c) Gamez, P.; Koval, I. A.; Reedijk, J. *Dalton Trans.* **2004**, 4079.
(3) (a) Bertini, I., Sigel, A., Sigel, H., Eds. *Handbook of Metalloproteins*; Marcel Dekker Inc.: New York, 2001. (b) Messerschmidt, A., Huber, R., Poulos, T., Wieghardt K., Eds. *Handbook of Metalloproteins*; J. Wiley & Sons: Chichester, UK, 2001.
(4) Stadtman, E. *Science* **1992**, *257*, 1220.
(5) (a) Brown, G. M.; Weaver, T. R.; Keene, F. R.; Meyer, T. *J. Inorg. Chem.* **1976**, *15*, 190. (b) Alvarez, V. E.; Allen, R. J.; Matsubara, T.; Ford, P. C. *J. Am. Chem. Soc.* **1974**, *96*, 7686. (c) Keene, F. R.; Meyer, T. *J. Am. Chem. Soc.* **1976**, *98*, 1884.
(6) (a) Lay, P. A.; Sargeson, A. M.; Skelton, B. W.; White, A. H. *J. Am. Chem. Soc.* **1982**, *104*, 6161. (b) Lay, P. A.; McLaughin, G. M.; Sargeson, A. M. *Aust. J. Chem.* **1987**, *40*, 1267.
(7) (a) Ugalde-Saldívar, V. M.; Sosa-Torres, M. E.; Ortiz-Frade, L.; Bernès, S.; Höpfl, H. *J. Chem. Soc., Dalton Trans.* **2001**, 3099. (b) Ugalde-Saldívar, V. M.; Sosa-Torres, M. E.; González, I. *Eur. J. Inorg. Chem.* **2003**, 978.

10.1021/ic8016968 CCC: $40.75
Published on Web 01/05/2009

Scheme 1. Ligands

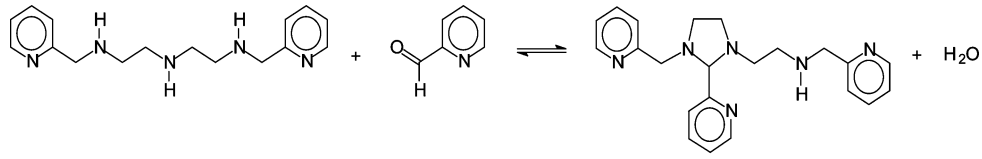

L^1 **L^2**

L^1 = 1,9-bis(2'-pyridyl)-2,5,8-triazanonane

L^2 = 1-[3-aza-4-(2-pyridyl)-butyl]-2-(2-pyridyl)-3-[(2-pyridyl)-methyl]imidazolidine

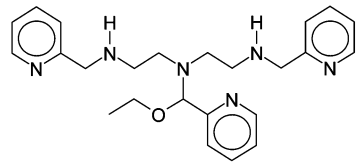

L^3 =1,9-bis(2'-pyridyl)-5-[(ethoxy-2''-pyridyl)methyl]-2,5,8-triazanonane

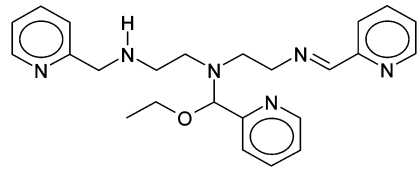

L^4 = 1,9-bis(2'-pyridyl)-5-[(ethoxy-2''-pyridyl)methyl]-2,5,8-triazanon-1-ene

we studied the conversion of the Fe(III) complex of the hexadentate amine ligand $\mathbf{L}^3$ = 1,9-bis(2″-pyridyl)-5-[(ethoxy-2′-pyridyl)methyl]-2,5,8-triazanonane and the subsequent oxidation and electron transfer steps.[8] Several mechanistic studies of metal-promoted dehydrogenation reactions of amines[9−12] have been published. Note that these systems usually required an additional oxidant to start the reaction and that two different imines were produced as a result of the oxidative dehydrogenation.[13,14] For structurally well-defined iron complexes with polydentate amines, detailed mechanistic studies have not been formulated so far.

In this contribution, we propose a mechanism for the oxidative dehydrogenation reaction of $[Fe(III)L^3]^{3+}$(**1**) in ethanol in the absence of dioxygen, which is consistent with the experimentally determined rate law. Ethanolic buffer solutions, with 2,4,6-trimethylpyridine as a base (pK_a = 9.48 ± 0.05, 25 °C) proved to be an excellent medium to study the reaction. Furthermore, the X-ray structure of the reaction product, the kinetically stable complex $[Fe(II)L^4]^{2+}$, $\mathbf{L}^4$ = 1,9-bis(2′-pyridyl)-5-[(ethoxy-2″-pyridyl)methyl]-2,5,8-triazanon-1-ene (**2**), has been solved. Complex **2** carries one imine function, and it has a non-centrosymmetric symmetry thus being chiral.

Experimental Section

Syntheses. For details of the ligand structures, refer to Scheme 1. 1,9-Bis(2′-pyridyl)-2,5,8-triazanonane trihydrochloride, **L^1·3HCl**, 1-[3-aza-4-(2-pyridyl)butyl]-2-(2-pyridyl)-3-[(2-pyridyl)methyl]imidazolidine ($\mathbf{L}^2$), and $[Fe(III)(DMSO)_6](NO_3)_3$ used for the synthesis of **1** and **2** were prepared by procedures published elsewhere.[8,15,16] The ^{1}H NMR spectrum of $\mathbf{L}^1$ in D_2O corresponded to the reported one.[15b] 1,9-Bis(2′-pyridyl)-5-[(ethoxy-2″-pyridyl)methyl]-2,5,8-triazanonane ($\mathbf{L}^3$) and $[Fe(III)L^3]^{3+}$ (**1**) were prepared by mixing solutions of $\mathbf{L}^2$ (10^{-4} M) and $[Fe(III)(DMSO)_6](NO_3)_3$ (2×10^{-4} M) in ethanol.[7]

$[Fe(II)L^4][BPh_4]_2$, {1,9-bis(2′-pyridyl)-5-[(ethoxy-2″-pyridyl)methyl]-2,5,8-triazanon-1-ene}-iron(II) bis(tetraphenylborate) (**2**). This complex was synthesized earlier;[7] however, no crystal structure had been determined when the product was isolated from those starting materials. So, we proceeded to crystallize this compound. When the final product **2** was recrystallized, two different forms

(8) Ugalde-Saldìvar, V. M.; Farfán, N.; Toscano, A. R.; Höpfl, H.; Sosa-Torres, M. E. *Inorg. Chim. Acta* **2005**, *358*, 3545.
(9) (a) Goto, M.; Takeshita, M.; Kanda, N.; Sakai, T.; Goedken, V. *Inorg. Chem.* **1985**, *24*, 582. (b) Barefield, E. K.; Mocella, M. T. *J. Am. Chem. Soc.* **1975**, *97*, 4238.
(10) Diamond, S. E.; Tom, G. M.; Taube, H. *J. Am. Chem. Soc.* **1975**, *97*, 2661.
(11) Ridd, M. J.; Keene, F. R. *J. Am. Chem. Soc.* **1981**, *103*, 5733.
(12) Liu, S.; Lee, S.; Wang, S.; Yeh, A.; Gau, H.-M.; Shao, M.-Y. *Inorg. Chem.* **2001**, *40*, 6139.
(13) (a) Keene, F. R.; Ridd, M. J.; Snow, M. R. *J. Am. Chem. Soc.* **1983**, *105*, 7075. (b) da Costa Ferreira, A. M.; Toma, H. E. *J. Chem. Soc., Dalton Trans.* **1983**, 2051. (c) Kuroda, Y.; Tanaka, N.; Goto, M.; Sakai, T. *Inorg. Chem.* **1989**, *28*, 2163.
(14) Mahoney, D. F.; Beattie, J. K. *Inorg. Chem.* **1973**, *12*, 2561.
(15) (a) Raleigh, C. J.; Martell, A. E. *Inorg. Chem.* **1985**, *24*, 142. (b) Harris, W. R.; Murase, I.; Timmons, J. H.; Martell, A. E. *Inorg. Chem.* **1978**, *17*, 889. (c) Ugalde-Saldívar, V. M.; Luna-Canut, A.; Sosa-Torres, M. E.; Rosales-Hoz, M. J.; Toscano, A. R.; Tobe, M. L. *J. Chem. Soc., Dalton Trans.* **1990**, 3629.
(16) Langford, C. H.; Chung, F. M. *J. Am. Chem. Soc.* **1968**, *90*, 4485.

of purple crystals were obtained: rectangular prisms that correspond to the chemically and structurally characterized, $\mathbf{2_r}$,[7] and octahedral prisms $\mathbf{2_{Oh}}$. Elemental analysis of these latter crystals: C, 77.21%; H, 6.55%; N, 7.55%; $C_{72}H_{70}B_2FeN_6O$, M = 1112.81, requires C, 77.71%; H, 6.34%; N, 7.55%). IR (KBr): 3242m [ν(NH)], 2982m [$\nu(CH_2)$], 1604m [$\nu(C{=}N_{ar})$], 1578m [$\nu(C{=}C)$], 1324m [$\delta_{sym}(CH_3)$], 1091s [$\nu(C{-}O)$] cm^{-1}.

Instrumentation and Methods. Fourier transform infrared spectra over the range 4000−200 cm^{-1} of the complexes (KBr pellets) were obtained on a Perkin−Elmer 599-B instrument. Electronic absorption spectra were recorded on a Hewlett-Packard 8452 diode array spectrophotometer. The ^1H and ^{13}C NMR spectra were measured in acetone-d_6 on a Varian NMR Unity Plus 500 and a Varian 300 NMR Unity-Inova spectrometer, with TMS as internal standard. Elemental analyses of C, H, and N were carried out with a Fisons Instrument EA 1108. Magnetic susceptibilities were determined on a Faraday balance at room temperature; the system was calibrated against $Hg[Co(SCN)_4]$.

Determination of pH* in Ethanol. An Orion 720A pH meter, equipped with a combined glass electrode, was used to determine the pH* in ethanol at different temperatures; the reference electrode was Ag−AgCl in saturated LiCl/ethanol. The system was calibrated against two standards in ethanol, at 25 °C:[17] pH* 5.02, 2.55 mM HCl, and 10.19 mM NaCl; pH* 9.95, 25.5 mM acetic acid, 12.75 mM sodium acetate, 6.38 mM NaCl. To get accurate pH* values at the working temperature, we obtained the pH* and the temperature coefficients for both standards and calibrated the system at 60 °C; experimental details will be published elsewhere.[18]

Determination of the pK_a of 2,4,6-trimethylpyridine in ethanol. Freshly distilled 2,4,6-trimethylpyridine (0.5 M final concentration) was dissolved in absolute ethanol; an aliquot of this solution was titrated at 25 °C with a 0.3 M solution of hydrochloric acid to give a pK_a value of 9.48 ± 0.05 (determined in triplicate).

Preparation of the Buffers in Ethanol. Buffers were prepared by dissolving 2,4,6-trimethylpyridine in ethanol and adding the appropriate amount of hydrochloric acid until the desired pH* had been reached. A 0.5 M 2,4,6-trimethylpyridine buffer solution was titrated both with a hydrochloric acid and with a lithium hydroxide standard solution to determine the buffer capacity, which resulted as pH* = pK_a ± 1. The concentration of EtO^- was calculated from $[EtO^-] = 10^{(\log K^T_{EtOH} + pH)}$; K^T_{EtOH}, the ionic product of ethanol was obtained from the literature,[19] and NaCl was used to maintain the ionic strength μ at 0.01 M.

Kinetic Measurements. The reactions were followed spectrophotometrically in a thermostatted 1.0 cm^3 cell (60 ± 0.1 °C). Spectra were recorded over the range 190−820 nm, and the rate constants were determined from the change in absorbance at fixed wavelength with time. Plots of ln $|A_t - A_\infty|$ vs time were linear; slope = k_{obs}; A_t and A_∞ represent the absorbances at time t and at the end of the reaction, respectively; A_∞ was determined after 10 half-lives.

The overall process consisted of two reactions. First, the starting complex **1** was formed by a rapid reaction, by mixing solutions of $\mathbf{L}^2$ (10^{-4} M) and $[Fe(III)(DMSO)_6](NO_3)_3$ (10^{-4} M) in ethanol. The reaction was followed over the pH* range 7.92−9.21, at 60 ± 0.1 °C, under nitrogen atmosphere at 344 nm. The following oxidative dehydrogenation reaction was slower and started immediately once **1** was formed. It was followed at 374 nm (Figure 3) and led to the Fe(II)-monoimine complex **2**, under our experimental conditions. The observed first- and second-order rate constants were calculated taking into account the K_{EtOH} at this ionic strength and temperature.

Determination of the kinetic isotope effect in the oxidative dehydrogenation of **1**. The deuterated form of $\mathbf{L}^2$ (L^2-ND) was prepared by dissolving $\mathbf{L}^2$ (L^2-NH) in a 1:1 mixture of $C_2H_5{-}OD$ (99.5% D) and D_2O (99.9% D); this solution was evaporated to dryness on a steam bath (process repeated three times). The deutero buffer was prepared by dissolving 2,4,6-trimethylpyridine in $C_2H_5{-}OD$ and adding the appropriate amount of DCl until pH* = 9.52 was reached. The kinetic isotope effect was determined by comparing the first-order rate constants for the oxidative dehydrogenation of the normal complex **1** in buffer (H_2O) and the deuterated complex **1** in buffer (D_2O) under identical experimental conditions of temperature, pH*, and ionic strength.

X-ray Analysis. A dark purple crystal of $\mathbf{2_{Oh}}$ (octahedral form) was mounted on a glass fiber and transferred to a Siemens P4/PC diffractometer with graphite-monochromated Mo Kα (λ= 0.71073 Å) radiation. Data were collected at 293 K. The structure was solved by direct methods and was refined against F2 with the program SHELXTL 4.[20]

Crystal data of $\mathbf{2_{Oh}}$ ($C_{72}H_{70}B_2FeN_6O$): orthorhombic, a = 17.351(2), b = 17.582(4), c = 20.461(3) Å, U = 6241.9(18) $Å^3$, T = 293(2) K, space group $P\,2_12_12_1$ (no. 19), Z = 4, μ(Mo Kα) = 0.29 mm^{-1}, 6043 reflections measured, 6043 unique which were used in all calculations. The final $wR(F^2)$ was 0.1937 ($I > 2\sigma(I)$). Flack's parameter 0.11 (5). CCDC reference number 286407.

Results and Discussion

As a part of our ongoing research to unravel the mechanism of the transition metal-dependent oxidative dehydrogenation of amines, we investigated the reaction between the imidazolidine ligand $\mathbf{L}^2$ and $[Fe(III)(DMSO)_6](NO_3)_3$. The starting complex **1** was formed rapidly by mixing solutions of $\mathbf{L}^2$ and $[Fe(III)(DMSO)_6](NO_3)_3$ in ethanol (this is a labile species, which transforms to $[Fe(III)(EtOH)_6]^{3+}$) under the exclusion of oxygen. The formation of **1** was fast compared to the second reaction and did not depend on pH (7.92−9.21). Earlier, we had already shown by cyclic voltammetry that the opening of $\mathbf{L}^2$ led to the formation of the hexacoordinated $[Fe(III)L^3]^{3+}$ compound.[8] However, no spectroscopic study had been carried out to follow this reaction. Thus, shortly after mixing $\mathbf{L}^2$ and the Fe(III) complex, the UV/vis spectrum of the solution showed absorption maxima at λ_1 = 582 nm (ε = 204 M^{-1} cm^{-1}) and λ_2 = 390 nm (ε = 1870 M^{-1} cm^{-1}), which is assigned to **1**. This complex did not react with oxygen in acidic medium in line with its electrochemical properties ($E_{1/2}$ = −0.428 V vs Fc^+/Fc).[8] Once complex **1** had been formed, the actual oxidative dehydrogenation started, leading to the purple compound **2**. At the end of the reaction, **2** could be obtained by precipitating and filtering it. When this product was recrystallized from acetone, octahedral prisms $\mathbf{2_{Oh}}$ were obtained in contrast to the rectangular prisms $\mathbf{2_r}$[7a] obtained previously, when the dehydrogenation reaction was carried out with a pentadentate starting ligand. Both crystallographic forms of the compound were diamagnetic, i.e., the Fe(III)

(17) Galster H. *pH Measurement: Fundamentals, Methods, Aplications, Instrumentation*; VCH: Weinheim, 1991.
(18) Saucedo-Vázquez, J. P.; Sosa-Torres, M. E. to be submitted for publication.
(19) Bates. R. G. *Determination of pH, Theory, and Practice*; John Wiley & Sons: New York, 1973.
(20) Sheldrick G. M. *SHELXTL (Version 6.10)*; Bruker AXS Inc.; Madison, WI, 2000.

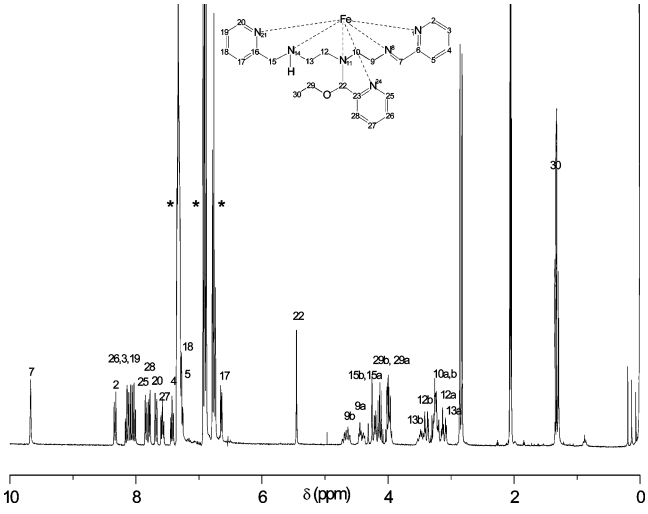

Figure 1. ^{1}H NMR spectrum in acetone-d_6 for $\mathbf{2_{Oh}}$ cation: $[Fe(II)L^4]^{2+}$ (300 MHz) at 298 K. TMS as internal reference; the resonances (*) arise from the counterion.

center in the starting complex **1** must have been reduced, and the coordinated polyamine ligand must have been oxidized to yield the corresponding Fe(II)-imine **2**. The ^{1}H and ^{13}C NMR assignments for $\mathbf{2_{Oh}}$ were achieved by 2D correlated COSY and HETCOR experiments (Figure 1). The well-resolved NMR spectra confirmed the diamagnetic nature of this product in solution and the formation of the imine function with chemical shifts of $\delta = 9.67$ and 170.61 ppm for H-7 and C-7, respectively. The hemiaminal function at carbon C-22 was identified by the chemical shifts of $\delta =$ 5.45 ppm for H-22, and $\delta = 99.53$ ppm for C-22. As C-22 is an asymmetric center, the neighboring methylene groups become diastereotopic (Table 1). The UV/vis spectrum of $\mathbf{2_{Oh}}$ in acetonitrile showed intense absorption maxima at 392 nm (8277 M^{-1} cm^{-1}) and 574 nm (6992 M^{-1} cm^{-1}). The magnitude of the extinction coefficients indicates that the d−d transitions in this region of the spectrum are masked by metal→ligand charge transfer transitions usually observed in complexes with unsaturated ligands.[21]

X-ray Structure of $\mathbf{2_{Oh}}$. In order to confirm the molecular structure of $\mathbf{2_{Oh}}$ determined by NMR, its structure was also determined by X-ray crystallography. The crystallographic and geometric parameters of the purple crystals of this octahedral form are summarized in Table 2. These data clearly document the presence of Fe(II) in $\mathbf{2_{Oh}}$, and the short distance of the C7−N8 bond (1.269 Å) undoubtedly confirms the presence of the imine moiety (Table 2). The ligand employs three pyridine nitrogens (N1, N21, N24), one imine nitrogen (N8), and two *tert*- and *sec*-amine nitrogens (N11 and N14), respectively, to bind Fe (II) (Figure 2). The Fe−N bond lengths cover the rather narrow range 1.96−2.02 Å compared to the broad range of 82−97° observed for the *cis* N−Fe−N angles, which mainly results from stereochemical constraints imposed by the ligand. The N11−Fe−N24 and N11−Fe−N21 angles show the largest deviation from 90°, i.e., 82.4° and 97.4°, respectively. Some lengthening of the Fe−N(pyridine) bond in **2** presumably arises from a stronger *trans* influence of the imine nitrogen atom compared to the *sec*- or *tert*-amine nitrogen atoms. The crystal structure (Figure 2) shows an ethoxy group bound to the carbon atom C22. Since the two arms of the ligand are inequivalent,

(21) (a) McMillin, D. R. In Electronic Absorption Spectroscopy, In *Physical Methods in Bioinorganic Chemistry*; Que, L., Jr., Ed.; University Science Books: Sausalito, CA, 2000; p 25. (b) Huheey, J. E.; Keiter, E. A.; Keiter, R. L. *Inorganic Chemistry, Principles of Structure and Reactivity*, 4th ed.; Harper Collins College Publishers: New York, 1993; p 459.

Table 1. ^{1}H and ^{13}C NMR Data, In Acetone-d_6, for $\mathbf{2_{Oh}}$ and $\mathbf{2_r}$ (500 MHz) at 298 K[a]

assignation	^{1}H NMR		^{13}C NMR		
nucleus	δ (ppm)	δ (ppm)	nucleus	δ (ppm)	δ (ppm)
H30	1.32	1.30	**C30**	15.87	15.87
H13a	3.11	3.00	**C10**	56.03	56.04
H12a	3.13	3.13	**C13, C9**	58.94	58.94
H10a,b	3.26	3.17	**C12**	60.40	60.43
H12b	3.39	3.19	**C15**	60.67	60.69
H13b	3.48	3.37	**C29**	70.19	70.19
$_{14}$NH	3.99	3.83	**C22**	99.53	99.55
H29a	3.99	3.94	**$C_p(\phi B_4)$**	122.35	122.33
H29b	4.12	4.08	**C25**	123.44	123.43
H15a	4.25	4.11	**C20**	125.90	125.90
H15b	4.28	4.18	**$C_m(B\phi_4)$**	126.09	126.09
H9a	4.42	4.30	**C27**	127.08	127.07
H9b	4.66	4.56	**C4**	127.27	127.26
H22	5.45	5.38	**C18**	127.74	127.74
H17	6.64	6.59	**C2**	129.15	129.15
$H_p(B\phi_4)$	6.76	6.74	**$C_o(B_4\phi)$**	137.09	137.08
$H_m(B\phi_4)$	6.91	6.89	**C3**	137.79	138.00
H18	7.26	7.21	**C19**	139.53	139.53
H5	7.28	7.23	**C26**	139.59	139.57
$H_o(B\phi_4)$	7.33	7.31	**C28**	153.19	153.19
H4	7.43	7.36	**C17**	154.58	154.58
H27	7.58	7.52	**C5**	155.44	155.44
H20	7.68	7.64	**C6**	163.47	163.50
H28	7.78	7.73	**$C_i(B_4\phi)$**	165.04	165.03
H25	7.84	7.77	**C23**	164.53	164.45
H19	8.03	7.98	**C_i $(B_4\phi)$**	165.04	165.03
H3	8.08	8.02	**C_i $(B_4\phi)$**	165.04	165.03
H26	8.14	8.08	**C_i $(B\phi_4)$**	165.04	165.03
H2	8.33	8.25	**C16**	166.85	166.89
H7	9.67	9.55	**C7**	170.61	170.59

[a] ref 7a. δ = chemical shift; *ortho* ($_o$), *meta* ($_m$), and *para* ($_p$).

Table 2. Selected Bond Lengths (Å) and Angles (°) for Compounds $\mathbf{2_r}$ and $\mathbf{2_{Oh}}$

bonds lengths (Å)	$\mathbf{2_r}$ [a]	$\mathbf{2_{Oh}}$
Fe(1)−N(21)	1.977(9)	1.989(8)
Fe(1)−N(14)	2.007(8)	2.023(8)
Fe(1)−N(11)	2.007(9)	2.020(9)
Fe(1)−N(8)	1.853(9)	1.867(10)
Fe(1)−N(1)	1.946(9)	1.960(8)
Fe(1)−N(24)	1.942(9)	1.954(9)
N(8)−C(7)	1.271(14)	1.269(16)
bond angles (°)	**$\mathbf{2_r}$ [a]**	**$\mathbf{2_{Oh}}$**
N(21)−Fe(1)−N(14)	83.0(5)	82.9(4)
N(21)−Fe(1)−N(11)	97.9(4)	97.5(4)
N(14)−Fe(1)−N(11)	86.1(4)	86.8(4)
N(21)−Fe(1)−N(8)	172.9(5)	173.2(4)
N(14)−Fe(1)−N(8)	90.8(4)	90.8(4)
N(11)−Fe(1)−N(8)	84.7(5)	84.8(4)
N(21)−Fe(1)−N(1)	96.0(5)	95.4(4)
N(8)−Fe(1)−N(1)	81.6(6)	82.3(4)
N(21)−Fe(1)−N(24)	93.1(5)	93.0(4)
N(14)−Fe(1)−N(24)	166.6(6)	167.8(4)
N(11)−Fe(1)−N(24)	81.8(6)	82.4(4)
N(8)−Fe(1)−N(24)	94.0(4)	93.6(4)
N(1)−Fe(1)−N(24)	97.9(6)	97.1(4)
C(9)−N(8)−Fe(1)	120.2(10)	118.1(9)
C(7)−N(8)−Fe(1)	118.5(12)	118.2(9)

[a] ref 7a.

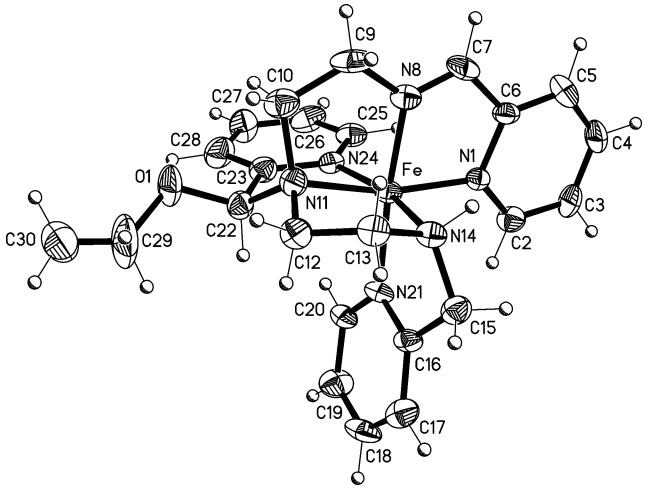

Figure 2. Structure of the $\mathbf{2_{Oh}}$ cation: $[Fe(II)L^4]^{2+}$, thermal ellipsoids with 20% probability.

carbon atom C22 will be chiral. Complex $\mathbf{2_{Oh}}$, which had been prepared by recrystallization of a racemic mixture of $\mathbf{2_r}$, contained the *R* isomer, probably by spontaneous resolution during crystallization. For the previously published structure of complex $\mathbf{2_r}$ (rectangular prisms)[7a] the asymmetric unit of the monoclinic cell contained two crystallographic independent cations and four tetraphenyl borate counterions, in the achiral monoclinic space group $P2_1/c$. In contrast, the new crystalline form of $\mathbf{2_{Oh}}$ has only one cation and two counterions with $Z = 4$ in the unit cell, with an orthorhombic noncentrosymmetric space group $P2_12_12_1$, which corresponds to a chiral compound. The bond lengths and angles of both crystalline forms of **2** (Table 2) are almost identical. The found magnetic susceptibility of **2** was negative and therefore the compound diamagnetic. On the other hand, the well-resolved NMR spectra of **2**, confirmed its diamagnetism in solution, confirming the low-spin state of the iron(II) of the product.

Mechanism of Oxidative Dehydrogenation. The iron-promoted dehydrogenation of the amine ligand requires the removal of two electrons and two protons. Two different pathways can be envisaged for the subsequent intramolecular redox process in which the metal is reduced and the ligand oxidized. The first mechanism involves two consecutive one-electron oxidations of the ligand coupled to proton removal, thus proceeds via radical intermediates. The second mechanism consists of a two-electron ligand-to-metal transfer, which may proceed either via hydride transfer or via proton abstraction followed by a two-electron transfer.

Oxidative Dehydrogenation of 1. Upon mixing stoichiometric amounts of ethanolic solutions of either Fe(III) or Fe(II), and of the polydentate amine ligand $\mathbf{L}^2$, the formation of intermediate species and the final product **2** could be followed by electrochemical methods.[8] Cyclic voltammetry allowed assignment of the individual redox states of the complexes formed in solution and clearly demonstrated an intramolecular redox process between Fe(III) and the amine ligand in **1** as described by the following disproportionation (eq 1):

$$2[Fe(III)L^3]^{3+} \rightarrow [Fe(II)L^4]^{2+} + [Fe(II)L^3]^{2+} + 2H^+ \quad (1)$$

The oxidation of the coordinated amine $\mathbf{L}^3$ leads to the unsaturated ligand $\mathbf{L}^4$. The insertion of the C=N double bond requires the release of two electrons, which are used to reduce Fe(III) to Fe(II) and form two different Fe(II) complexes (eq 1). This reaction depends on the pH of the reaction medium. At acidic pH*, the disproportionation of **1** does not occur, whereas at neutral and slightly basic pH*, the oxidative dehydrogenation and formation of the Fe(II) complexes **2** and $[Fe(II)L^3]^{2+}$ (**3**) is favored as outlined in Scheme 2.

In order to establish the dynamic behavior of the disproportionation reaction of **1**, and to determine the rate law, it was crucial to develop a reaction medium with suitable acid−base properties to keep the pH constant. Thus, several buffer solutions had to be tested including 2,4,6,-trimeth-

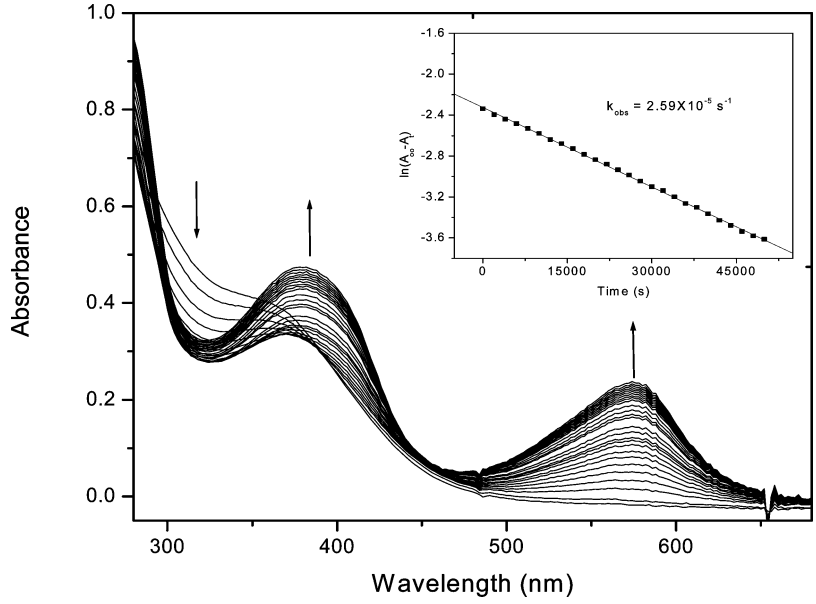

Figure 3. UV/vis spectra of the oxidative dehydrogenation of **1**: $[Fe(III)L^3]^{3+}$ in ethanol (60 °C; 30 min intervals; the decrease in absorbance at 300−350 nm results from the formation of **1**).

Scheme 2. General Outline of the Oxidative Dehydrogenation Reaction Including the Formation of $[FeL^3]^{3+}$ (eq 1) and the Disproportionation Reaction (eq 2)

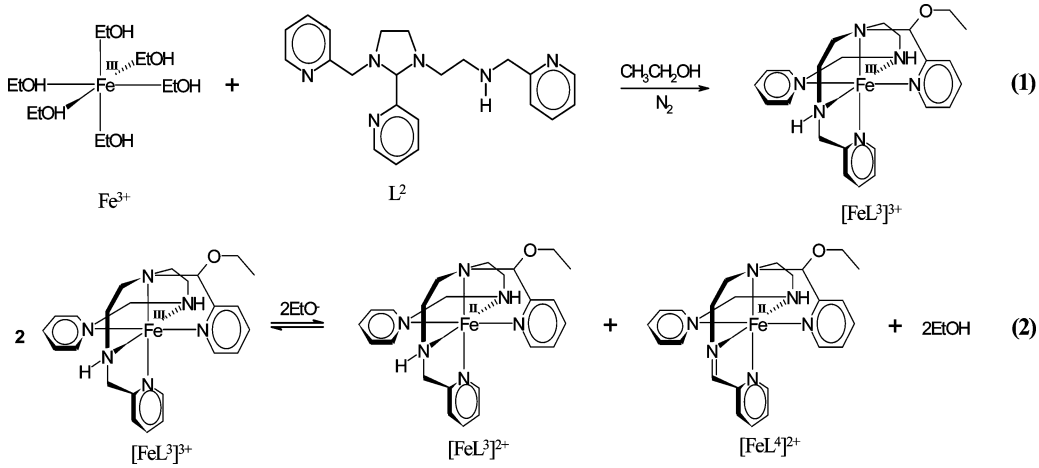

Table 3. Observed First-Order Rate Constants for the Formation of **1**, $[Fe(III)L^3]^{3+}$ (60 ° C, $\mu = 0.01$ M)

pH*	$10^5\ k_{obs}\ (s^{-1})$
7.92	3.13
8.34	3.25
8.99	3.09
9.21	3.35

ylpyridine in ethanol. We determined its pK_a to be 9.48 ± 0.05 (25 °C), and it proved to be an excellent medium to study the reaction spectrophotometrically.

The kinetics of the dehydrogenation were followed by UV/vis spectroscopy at 60 ± 0.1 °C, under a constant flow of dinitrogen, over the pH* range 7.92−9.21. The reaction was initiated by heating the ethanolic mixture of the starting imidazolidine ligand $\mathbf{L}^2$ and $[Fe(III)(DMSO)_6](NO_3)_3$ in a 1:1 stoichiometric ratio. First, in a rapid reaction, complex **1** was formed, with absorption maxima at $\lambda_1 = 582$ nm and $\lambda_2 = 390$ nm. The observed rate constant for this first reaction is the mean of three kinetic runs (Table 3). The consecutive process was slower and had to be followed again under dinitrogen (Figure 3), since it was highly affected by dioxygen. The final optical spectrum was assigned to a 1:1 mixture of complexes **2** and **3**, with absorption maxima at $\lambda_1 = 575$ nm ($\varepsilon = 6984\ M^{-1}\ cm^{-1}$) and $\lambda_2 = 394$ nm ($\varepsilon = 8036\ M^{-1}\ cm^{-1}$), and $E_{ap} = 0.075$ and 0.158 V and $E_{1/2} = -0.428$ V.[8] To confirm this assignment, complex **3** was synthesized as a green solid from $FeCl_2$ and L^3, under dinitrogen. The synthetic product showed maxima at $\lambda_1 = 582$ nm ($\varepsilon = 302\ M^{-1}\ cm^{-1}$) and $\lambda_2 = 385$ nm ($\varepsilon = 2116\ M^{-1}\ cm^{-1}$), and $E_{1/2} = -0.409$ V vs Fc^+/Fc. Thus, the final UV/vis spectrum of the reaction is fully consistent with the assumption of a mixture of the two Fe (II) complexes **2** and **3**, confirming the disproportionation reaction described in eq 1.

When the green solution of **3** was exposed to air, it turned immediately purple, indicating that **3** was oxidized to the corresponding Fe(III) complex **1**, which hereafter was converted to the stable Fe(II) complex **2**. Note that $E_{1/2}$ for **1** was −0.428 V vs Fc^+/Fc, whereas **2** did not show a reversible redox behavior. In the specific case of our reaction, the formation of the C═N double bond is crucial for the stabilization of the Fe(II)

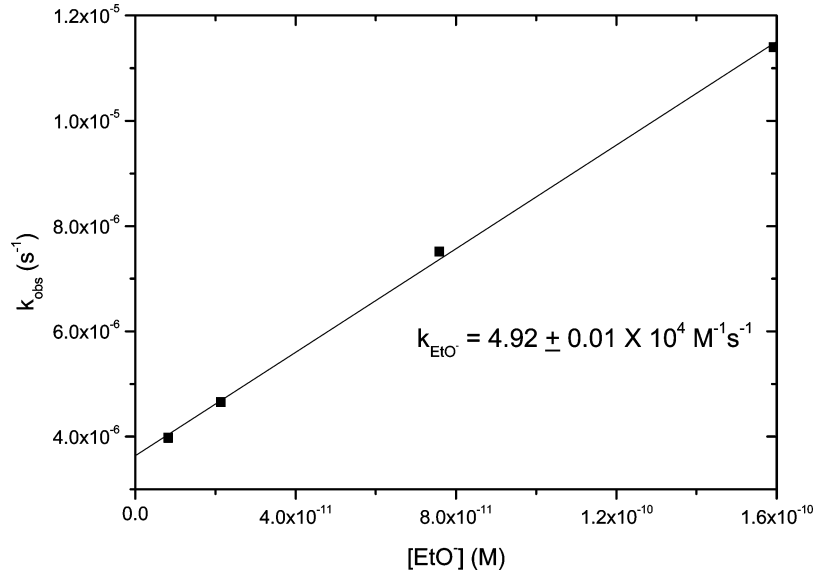

Figure 4. Determination of the second-order rate constant of the oxidative dehydrogenation of **1**: $[Fe(III)L^3]^{3+}$, in ethanol.

Table 4. Observed First-Order and Calculated Second-Order Rate Constants for the Oxidative Dehydrogenation of **1**, $[Fe(III)\ L^3]^{3+}$ (60 °C, $\mu = 0.01$ M)

pH*	10^{11} [EtO$^-$] (mol dm^{-3})	$10^6\ k_{obs}$ (s^{-1})	$10^{-4}\ k_{OH}$ (dm^3 mol^{-1} s^{-1})
7.92	0.83	3.98	4.84
8.34	2.13	4.66	5.05
8.99	7.58	7.52	5.19
9.21	15.92	11.4	4.91

oxidation state because of its strong π-acceptor capability, besides the conjugation in the system among the double bond C═N, aromatic ring, and iron(II) gives rise to an extraordinary stable coordinated complex, which is consistent with the high redox potential values, of the product, **2**, $E_{ap} = 0.075$ and $E_{ap} = 0.158$ V (versus Fc^+/Fc).[8] This is the reason the oxidative dehydrogenation of **1** did not produce a second imine, nitriles, or any carbonyl species.

Rate Law and Reaction Mechanism. The rate of the reaction was obtained over the pH* range 7.92−9.21 (Figure 4). The observed first-order rate constant, and the calculated second-order rate constants for this reaction are listed in Table 4.

From the experimental kinetic data measured under dinitrogen, the following second-order rate law was obtained (eq 2):

$$-\frac{d[Fe(III)L^3)^{3+}]}{dt} = k_{EtO^-}[Fe(III)L^3)^{3+}][EtO^-] \qquad (2)$$

We propose a three-step mechanism for the disproportionation reaction (eq 1), which includes the formation of two radical intermediates (eqs 3−5):

$$[(Fe(III)L^3)^{3+}] + [EtO^-] \underset{k_{-1}}{\overset{k_1}{\rightleftarrows}} [Fe(II)(L^{3\bullet})^{2+}] + EtOH \qquad (3)$$

$$[Fe(II)(L^{3\bullet})^{2+}] + [(Fe(III)L^3)^{3+}] \xrightarrow{k_2} [Fe(III)(L^{3\bullet})^{3+}] + Fe(II)(L^3)^{2+}] \qquad (4)$$

$$[Fe(III)(L^{3\bullet})^{3+}] + [EtO^-] \xrightarrow{fast} [Fe(II)(L^4)^{2+}] + [EtOH] \qquad (5)$$

The first step (eq 3) requires the deprotonation of a coordinated amine group in 1 which produces a first short-lived ligand-centered radical $[Fe(II)(L^{3\bullet})^{2+}]$. In the second step (eq 4), this radical intermediate reacts with a molecule of 1 to yield a second short-lived radical $[Fe(III)(L^{3\bullet})^{3+}]$. In the third step (eq 5), this second radical intermediate, after deprotonation, forms the imine complex **2** as the final product in a fast reaction.

Application of the steady-state approximation to the first putative radical intermediate leads to the following rate law (eq 6):

$$-\frac{d[(Fe(III)L^3)^{3+}]}{dt} = \frac{2k_1k_2[Fe(III)L^3)^{3+}]^2[EtO^-]}{k_{-1} + k_2[Fe(III)L^3)^{3+}]} \qquad (6)$$

With $k_2[(Fe(III)L^3)^{3+}] \gg k_{-1}$, eq 6 reduces to

$$-\frac{d[(Fe(III)L^3)^{3+}]}{dt} = 2k_1[Fe(III)L^3)^{3+}][EtO^-] \qquad (7)$$

Thus, the proposed reaction mechanism (eqs 3−5) is fully consistent with the experimentally determined rate law (eq 2). Under these conditions, the act of deprotonation becomes rate-determining, and thus, the studied system should be susceptible to general base catalysis and to a primary isotope effect.[22,23]

The rate of the oxidative dehydrogenation of **1** was studied at different concentrations of 2,4,6,-trimethylpyridine buffer, holding the ionic strength and the buffer ratio (hence the pH*) constant. The rate was found to increase with the concentration of base (Figure 5), and the rate law takes the form

$$-\frac{d[(Fe(III)L^3)^{3+}]}{dt} = [(Fe(III)L^3)^{3+}]\left(k_{EtO^-}[EtO^-] + \sum k_B[B]\right) \qquad (8)$$

The detection of general base catalysis is diagnostic of a process in which there is not a rapid, reversible, pre-equilibrium proton transfer, and it is consistent with the observed primary isotope effect $k_{EtO^-}{}^H/k_{EtO^-}{}^D = 1.73$ ($k_{obs}{}^H$

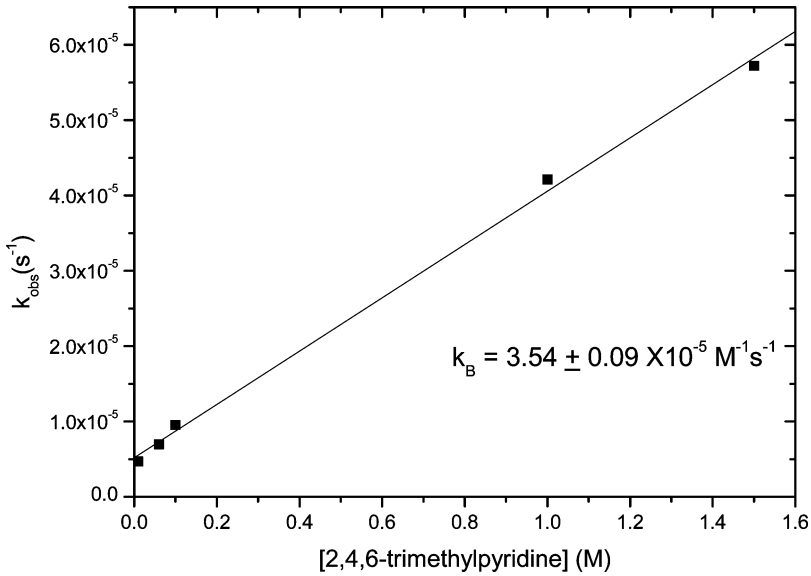

Figure 5. Determination of the second-order rate constant for the oxidative dehydrogenation of **1**: $[Fe(III)L^3]^{3+}$, as a function of 2,4,6-trimethylpyridine concentration in ethanol.

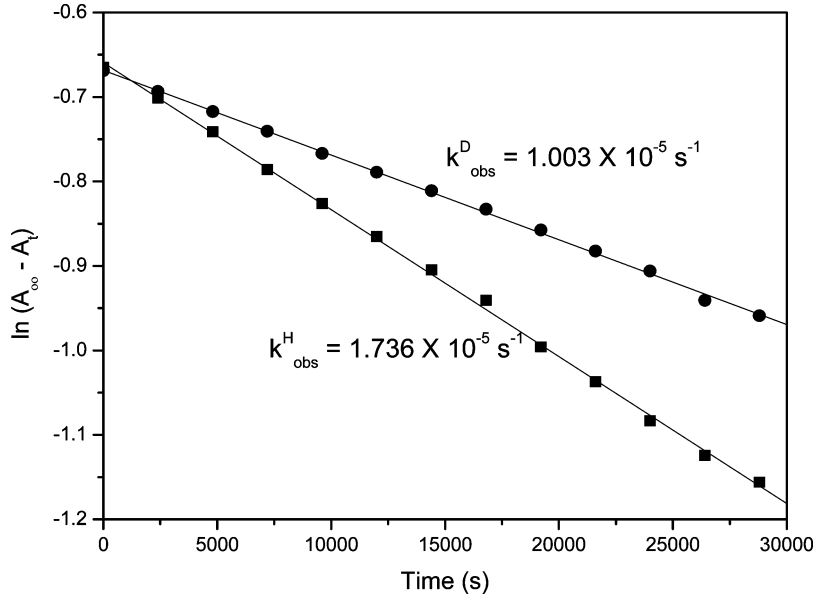

Figure 6. Determination of the primary kinetic isotope effect of the oxidative dehydrogenation of **1**: deutero -●-(ND) and protio -■-(NH) $[Fe(III)L^3]^{3+}$, pH* = 9.52, 60 °C, μ = 0.01 M; $k_{EtO^-}{}^{H}/k_{EtO^-}{}^{D} = 1.73$.

Scheme 3. Mechanistic View of the Oxidative Dehydrogenation Reaction[a]

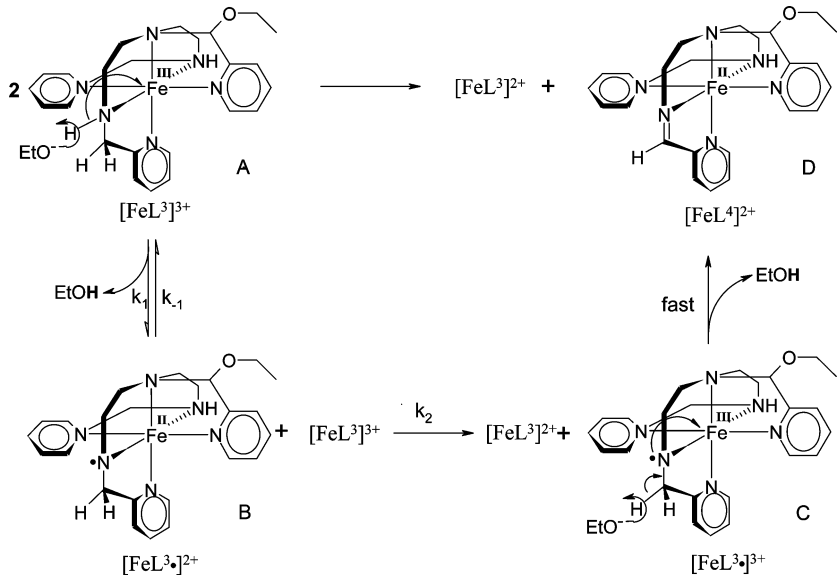

[a] The rate-limiting step includes the deprotonation of the N−H bond followed by single electron transfer to Fe(III) (state A) giving the Fe(II)-nitrogen radical complex (state B).

Table 5. Observed First-Order Rate Constants for the Oxidative Dehydrogenation of **1**, $[Fe(III)L^3]^{3+}$, with Varying Concentrations of 2,4,6-Trimethylpyridine (60 ° C, μ = 0.01 M).

[2,4,6,-trimethyl-pyridine] (M)	$10^6\ k_{obs}$ (s^{-1})
0.01	4.66
0.06	6.95
0.1	9.50
1.0	42.10
1.5	57.20

$= 1.736 \times 10^{-5}$ s^{-1} vs $k_{obs}{}^{D} = 1.003 \times 10^{-5}$ s^{-1}) for the oxidative dehydrogenation reaction of the normal (NH) and the deuterated (ND) form of $[Fe(III)L^{3+}]^{3+}$ (Figure 6). This isotope effect exhibits the same magnitude as those previously reported for amine coordination complexes reactions where deprotonation has been found to be a rate-limiting step.[22a,c]

These experimental findings represent the first kinetic demonstration that the proton transfer becomes rate-determining, followed by electron transfer, thus implicating a ligand-based radical intermediate in the oxidative dehydrogenation mechanism.

The types of radicals described here are highly reactive, but the electron deficiency on the nitrogen center can be stabilized either by electron-donating groups or by coordination to a transition metal ion.[24,25] In the latter case, the unpaired electron can be more discretely localized, either

(22) (a) Ahmed, E.; Tucker, M. L.; Tobe, M. L. *Inorg. Chem.* **1975**, 1. (b) Poon, C. K.; Tobe, M. L. *Chem. Commun.* **1968**, 156. (c) Lichtig, J.; Sosa, M. E.; Tobe, M. L. *J. Chem. Soc., Dalton Trans.* **1984**, 581. (d) Frost, A. A.; Pearson, R. G. *Kinetics and Mechanism. A Study of Homogeneous Chemical Reactions*, 2nd ed.; John Wiley and Sons, Inc.: New York, 1961, p 230.

on the nitrogen (aminyl) or on the metal (amidyl): LM^{m+}-$N^{\bullet}R_2 \leftrightarrows LM^{m+1}$-$N^{\bullet\bullet}R_2^{-}$. Recently, an aminyl radical has been reported that was stabilized as a rhodium(I) complex and its structure characterized by X-ray crystallography, electron paramagnetic resonance, and DFT calculations. Is it worth mentioning that this latter compound reacts with substrates X−H including thiophenol and the stannane Bu_3Sn−H. [26]

Conclusions

A mechanism for the oxidative dehydrogenation of a multidentate amine coordinated to iron(III) has been derived on the basis of both kinetic and structural data. The dehydrogenation reaction, under dinitrogen, proceeds via disproportionation of the Fe(III) complex **1** to yield two different Fe(II) complexes **2** and **3**. Thus, dehydrogenation of complex **1** requires both a metal-based and a ligand-based redox reaction (Schemes 2 and 3). Fe(II) complex **2** carries a C=N double bond as clearly shown by NMR spectroscopy and X-ray crystallography. The minimal reaction Scheme 3 proposed by us includes the formation of two short-lived radicals, with the unpaired electron most likely localized on the amine nitrogen next to the iron center (eqs 3−5). Application of the steady-state approximation to the first radical species, $[Fe(II)(L^{3\bullet})^{2+}]$ [(eq 3), leads to a rate law fully consistent with the experimental data obtained in this work. The observation of general base catalysis and a primary isotope effect in the oxidative dehydrogenation of **1** is in line with the assumption that in the system described here there is no rapid, reversible, pre-equilibrium proton transfer. On the contrary, the deprotonation of the polyamine Fe(III) complex becomes the rate-determining step, followed by electron transfer.

Acknowledgment. M.E.S.T. gratefully acknowledges the financial support provided by DGAPA-UNAM (research project IN210108); J.P.S.V. thanks CONACYT for a Ph.D. scholarship, and P.K. thanks the University of Konstanz for financial support (Kr 04/75).

Supporting Information Available: Crystallographic data. This material is available free of charge via the Internet at http://pubs.acs.org.

IC8016968

(23) (a) Tobe, M. L. In *Base Hydrolysis of Transition-Metal Complexes*; Sykes, A. G., Ed.; Vol. 2 in Advances in Inorganic and Bioinorganic Mechanisms; Academic Press: London, 1983; pp 8−10. (b) Marangoni, G.; Panayotou, M.; Tobe, M. L. *J. Chem. Soc., Dalton Trans.* **1973**, 1989. (c) Ahmed, E.; Tobe, M. L. *Inorg. Chem.* **1974**, *13*, 2956.
(24) Alfassi, Z. B., Ed. *N-Centered Radicals*; John Wiley & Sons: Chichester, 1998.
(25) Chaudhuri, P.; Wieghardt, K. *Prog. Inorg. Chem.* **2001**, *50*, 151.
(26) Büttner, T.; Geier, J.; Frison, G.; Harmer, J.; Calle, C.; Schweiger, A.; Schönberg, J.; Grützmacher, H. *Science* **2005**, *307*, 235.